RSC Advances

PAPER

View Article Online
View Journal | View Issue

Cite this: *RSC Adv.*, 2021, **11**, 17391

DFT insight into the effect of Cu atoms on adsorption and dissociation of CO_2 over a $Pd_8/TiO_2(101)$ surface†

Li Liu *[ab] and Pingli Lv[bc]

Received 4th March 2021
Accepted 5th May 2021

DOI: 10.1039/d1ra01724a

rsc.li/rsc-advances

In order to improve the photocatalytic activity of a bimetallic cocatalyst, understanding its mechanism is very important for the development of a CO_2 photocatalyst. In this study, density functional theory (DFT) calculations were performed to investigate CO_2 adsorption and dissociation over Pd–Cu bimetallic clusters loaded on a $TiO_2(101)$ surface, aiming at understanding the origin of the effect caused by the presence of Cu. The results demonstrated that the introduction of a Cu atom has a dual effect on the adsorption and dissociation of CO_2: (1) it provides the positive polarization charge center to enhance CO_2 adsorption, and (2) it up-shifts the d-band center of the Cu atom to improve the activation of CO_2. Thus, the activity of the $Pd_7Cu_1/TiO_2(101)$ surface, as compared with that of the $Pd_8/TiO_2(101)$ surface, can be significantly improved, and the active center is the introduced Cu atom. This result is not only helpful for the development of effective CO_2 photocatalysts but also crucial to understand the basic mechanism of bimetallic catalysis.

1. Introduction

In recent decades, the significant increase in the amount of carbon dioxide (CO_2) in the atmosphere has been widely regarded as a global environmental problem.[1] Therefore, extensive research has been carried out to reduce CO_2 levels. In particular, the photocatalytic reduction of CO_2 into hydrocarbon fuels and chemicals is considered an effective method of controlling and utilizing CO_2.[2–4] Photocatalytic CO_2 reduction by H_2O was first reported more than 30 years ago and is currently gaining more attention, because sunlight can be used as the primary energy source for this reduction. There have been many studies on CO_2 photoreduction, and various materials (especially semiconductors) have been evaluated for this purpose.[2–7] Among all types of semiconductors, TiO_2 has been the most commonly used photocatalyst because of its many advantages, including chemical and thermal stability, abundance, low toxicity, low cost, and high UV photoactivity.[8–10]

Although TiO_2 is the most explored semiconductor for the photocatalytic reduction of CO_2, its efficiency is still far from optimal due to the lack of visible light photoreaction, rapid electron–hole recombination of photogenerated charges, and inefficient CO_2 capture.[11,12] The combination of TiO_2 and other active ingredients is expected to overcome these limitations. In the past few decades, noble metals, such as Au, Pt, Ag, Cu, and Pd, have been studied as cocatalysts to promote the capability of TiO_2 semiconductors in photocatalytic CO_2 activation and conversion.[11–18] In addition, bimetallic cocatalysts (such as PdCu, AuCu, CuPt, and AgPd, *etc.*) have higher CO_2 conversion activity than single metal nanoparticles (NPs).[11,12,16,19–25] For example, Garcia's group reported that Au and Cu loaded TiO_2 photocatalyst in the appropriate Au/Cu ratio is an extremely efficient material for the solar-light reduction of CO_2 to CH_4.[11] Tan *et al.* reported that the Ag/Pd bimetals supported on N-doped TiO_2 nanosheet exhibit high selectivity for CO_2 conversion.[12] Recently, Huang *et al.* reported that the efficiency of CO_2 hydrogenation to C_2H_5OH can be optimized by adjusting the composition of Pd–Cu NPs and catalyst support.[25] Long *et al.*[16] also indicated that isolated Cu atoms in a Pd lattice can form highly selective active sites for photocatalytic conversion of CO_2 to CH_4.

It has been established that bimetallic cocatalysts often exhibit better catalytic performance than their corresponding elemental metal counterparts due to their composition and synergic effects on the catalytic properties.[26] However, the mechanism for improving photocatalytic activity and selectivity of bimetallic cocatalysts remains unclear and needs further study. Furthermore, the photoreduction of CO_2 is a complex reaction process, mainly encompasses the following elementary steps: (i) photon absorption and excited carrier generation; (ii) activation of CO_2 to form $CO_2^{\delta-}$; (iii) dissociation of the C–O bond; and (iv) desorption of reduced products from the active

[a]State Key Laboratory of Biobased Material and Green Papermaking, Qilu University of Technology (Shandong Academy of Sciences), Jinan, 250353, China. E-mail: liuli_1636@qlu.edu.cn; Fax: +86 0531 89631630; Tel: +86 0531 89631168

[b]School of Light Industry and Engineering, Qilu University of Technology (Shandong Academy of Sciences), Jinan 250353, China

[c]School of Chemistry and Chemical Engineering, Shandong University, Jinan 250100, China

† Electronic supplementary information (ESI) available. See DOI: 10.1039/d1ra01724a

sites.[4] Among them, some of the main challenges have not been completely resolved, such as the complicated activation and adsorption mechanisms of CO_2, the mechanisms and pathways of photocatalytic reaction, and low efficiency and selectivity of different products.[13] Therefore, it is essential to use theoretical calculations to explain the role of bimetallic cocatalysts in enhancing the activity, selectivity and stability of semiconductor photocatalysts, and to provide theoretical basis for design of new, high-performance CO_2 reduction cocatalysts. In this study, we chose TiO_2(101) loaded with Pd–Cu bimetallic NPs, which is reported to be an effective catalyst for the photocatalytic reduction of CO_2,[16] to explore the catalysis of bimetallic nanoparticles, and to clarify how the presence of Cu atom improves the catalytic activity of Pd-loaded TiO_2(101) surface. The (101) surface of anatase was selected because this surface is the most stable. The calculation results indicates that the electronic structure of supported Pd–Cu clusters is very important to the catalytic performance. The strong positive polarization potential and the elevated Cu d-band center make Pd_7Cu_1 have higher activity on TiO_2(101), which promotes adsorption and dissociation of CO_2.

2. Computational methods

All of the DFT[27] calculations were carried out with the GGA-PBE[28–31] functional using the CASTEP package.[32] Electronic wave functions were expanded in a plane-wave basis set, and ultrasoft pseudopotentials were used to describe the ionic cores.[33] The cutoff energy was set to 400 eV, and the Monkhorst–Pack[34] k-points sampling was generated with a $2 \times 2 \times 1$ grid. In order to determine the activation barriers of CO_2 dissociation, the complete LST/QST method was used to search for the transition states.[35] To confirm the transition states, we performed nudged elastic band (NEB) calculations using TS confirmation.

It is well-known that the standard DFT calculation will greatly underestimate the band gap due to the insufficient cancellation of the self-interaction energy inherent in the DFT functional, which may affect the calculation results.[36–38] To investigate this possibility, we did the test calculations by using the DFT+U method for Pd_8 cluster on TiO_2(101) surface and CO_2 on Pd_8/TiO_2 (101) surface. $U = 3.5$ eV was chosen according to the literature.[36,39] It can be seen from Table S1 in ESI† that the charge distribution on the Pd_8 cluster calculated by DFT+U is similar to that calculated by DFT, and the adsorption stability trend of Pd_8/TiO_2(101) to CO_2 is consistent (see Fig. S1 in ESI†). Because we only focus on qualitative trend analysis, the DFT is used in the following calculation.

A six layer slab with a (3×3) supercell was adopted to simulate the TiO_2(101) surface. The Pd_8 cluster has been studied for a long time and widely reported in the literature. Previous DFT calculations have shown that the lowest energy structure of the free Pd_8 cluster has a bicapped octahedral geometry with D_{2d} symmetry.[40,41] Therefore, Pd_8 clusters with D_{2d} symmetry were used in this work, as shown in Fig. 1a. During the calculation, the three top layers and the adsorbates relaxed. A vacuum region of 15 Å was chosen for TiO_2(101). The free CO_2 molecule was optimized in a 10 Å × 10 Å × 10 Å unit cell. The optimized C–O bond length and O–C–O angle are 1.178 Å and 180.0°, respectively, which are consistent with the experimental[42] and theoretically[43] values reported previously.

The adsorption energy of CO_2 is calculated as follows:

$$E_{ads} = E_{CO_2 + surface} - [E_{CO_2} + E_{surface}]$$

where $E_{CO_2 + surface}$ represents the energy of the Pd–Cu/TiO_2(101) surface with the adsorbed CO_2, E_{CO_2} represents the energy of free CO_2, and $E_{surface}$ represents the energy of the Pd–Cu/TiO_2(101) surface.

3. Results and discussion

3.1. Pd_8 and Pd_7Cu_1 clusters on TiO_2(101)

In order to find the most stable configuration of Pd_8 on TiO_2(101) surface, we constructed various possible configurations (see Fig. S2 in ESI†). Through optimization, we found that the structure shown in Fig. 1 is the most stable. As for Pd_7Cu_1 on TiO_2(101) surface, we tested eight possible replacing modes in order to find the most stable configuration, as shown in Fig. S3.† We chose the most stable configuration for further research, as shown in Fig. 2. A comparison to the optimized Pd_8 cluster shows that the Pd–TiO_2(101) interactions result in a completely different structure. On TiO_2(101), the cluster

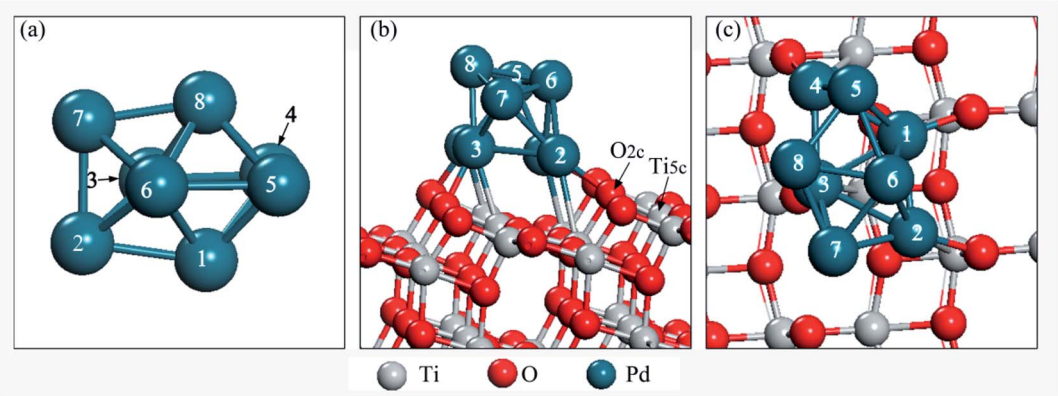

Fig. 1 (a) Pd_8 cluster, (b) side view of the Pd_8/TiO_2(101) surface, and (c) top view of the Pd_8/TiO_2(101) surface.

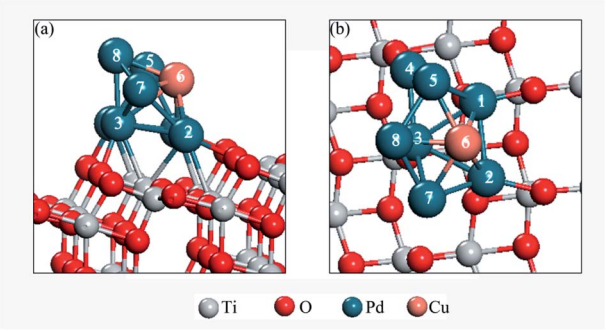

Fig. 2 The side (a) and top view (b) of the most stable model of the Pd_7Cu_1 cluster on the TiO_2(101) surface.

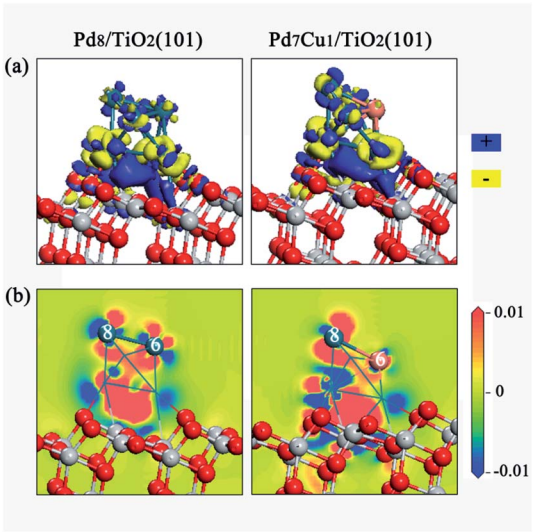

Fig. 3 Charge density difference for the Pd_8/TiO_2(101) (left) and Pd_7Cu_1/TiO_2(101) (right) surfaces.

adopts a bilayer structure. This is due to the fluxionality of the metal cluster.

The charge density difference and Mulliken charge analysis for the Pd_8/TiO_2(101) and Pd_7Cu_1/TiO_2(101) surfaces were calculated to further understand the interaction between the Pd_8 (or Pd_7Cu_1) cluster and the TiO_2 surface from the perspective of electronic structure. As shown in Fig. 3a, when Pd_8 or Pd_7Cu_1 clusters supported on the surface of TiO_2(101), obvious charge transfer occurs at the interface, which is a long-range interaction that affects the charge distribution of the Pd or Cu atoms in the upper layer, and can lead to charge polarization between the clusters and the TiO_2(101) surface. It can be seen from the electrostatic potential of Pd_8/TiO_2(101) and Pd_7Cu_1/TiO_2(101) in Fig. S4† that the polarization potentials of Pd_8 and Pd_7Cu_1 are positive, while the polarization potentials of TiO_2(101) surface are negative. Therefore, when the interface forms and reaches an equilibrium, the final polarized electric field is from the clusters to the TiO_2(101) surface.

As shown in Fig. 3b, although both the Pd_8 and Pd_7Cu_1 clusters can provide electrons to the TiO_2(101) surface, the charge transfer of each atom is different. Mulliken charge analysis also confirmed this conclusion. The results in Table 1 show that all interfacial Pd atoms (from Pd-1 to Pd-4) of the Pd_8 cluster are positively charged. However, all of the top-layered Pd atoms (from Pd-5 to Pd-8) are negatively charged. For the Pd_7Cu_1 cluster, because the electronegativity of Cu is lower than that of Pd, the Cu-6 can provide its electrons to the neighboring Pd atoms and become positively charged.

3.2. Adsorption and activation of CO_2 over Pd_8/TiO_2(101)

For the Pd_8/TiO_2(101) surface, the most stable CO_2 adsorption configuration is shown in Fig. 4a, labeled as Pd_8–CO_2. The other unstable adsorption models are displayed in Fig. S5.† We summarized our calculated results in Table 2. In order to describe conveniently, the two oxygen atoms of the CO_2 are labeled Oa and Ob, respectively.

In configuration Pd_8–CO_2 (Fig. 4a), CO_2 is adsorbed on Pd-6 and Pd-7 atoms in form of a bidentate carbonate, with an adsorption energy of −0.58 eV. The Oa bonds to the Pd-6 atom, and the C atom bonds to the Pd-7 atom. The bond lengths of Oa–Pd-6 and C–Pd-7 bonds are 2.175 Å and 2.004 Å, respectively. As shown in Table 2, compared with the free CO_2 molecule, the adsorbed CO_2 in configuration Pd_8–CO_2 has been heavily distorted. The length of the C–Oa and C–Ob bonds are both elongated, and the Oa–C–Ob angle is reduced to 141.7°, which indicates that CO_2 is activated. In addition, it can be seen from Table S2† that the adsorbed CO_2 has a negative charge of $-0.43|e|$, as a consequence of electron transfer from surface to CO_2, and leading to a bent anionic $CO_2^{\delta-}$ species. The $CO_2^{\delta-}$ can increase the reactivity of CO_2, including the breaking of C–O bond. Local density of states (LDOS) analysis was also conducted to further understand the interaction between the Pd_8/TiO_2(101) surface and adsorbed CO_2. Fig. S6a† shows the LDOS of free CO_2; Fig. S6b† shows the LDOS of Pd_8–CO_2 configuration. From Fig. S6b,† for C and Pd-7 (or Oa and Pd-6) atom in configuration Pd_8–CO_2, it can be clearly seen that the orbital overlap is more obvious in the range of −10 to 0 eV. This indicates that the interaction between the CO_2 and the Pd_8/TiO_2(101) is strong.

3.3. Adsorption and activation of CO_2 over Pd_7Cu_1/TiO_2(101)

For CO_2 adsorption on Pd_7Cu_1/TiO_2(101), the most stable adsorption configuration is shown in Fig. 4b, labeled as

Table 1 The Mulliken charges carried by Pd and Cu atoms on the Pd_8/TiO_2(101) and Pd_7Cu_1/TiO_2(101) surfaces

Pd_8/TiO_2(101)	Pd-1	Pd-2	Pd-3	Pd-4	Pd-5	Pd-6	Pd-7	Pd-8	Total
Charge/$\|e\|$	0.19	0.13	0.08	0.09	−0.10	−0.01	−0.08	−0.01	0.29
Pd_7Cu_1/TiO_2(101)	Pd-1	Pd-2	Pd-3	Pd-4	Pd-5	Cu-6	Pd-7	Pd-8	Total
Charge/$\|e\|$	0.17	0.16	0.14	0.04	−0.18	0.14	−0.10	−0.05	0.32

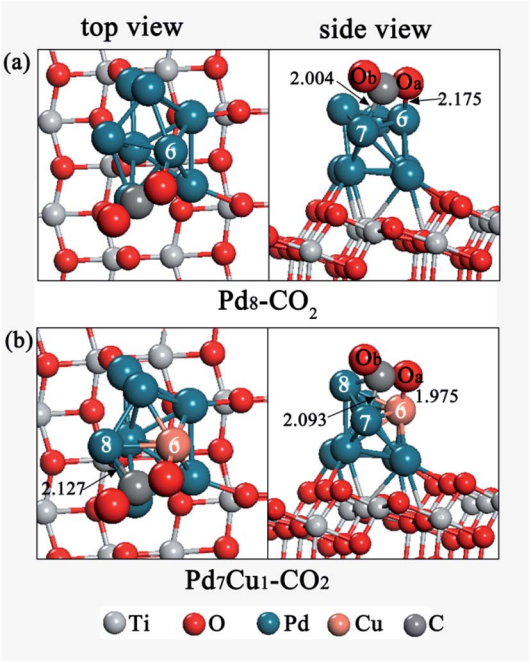

Fig. 4 Top and side views of CO_2 adsorption configuration on (a) the $Pd_8/TiO_2(101)$ surface and (b) the $Pd_7Cu_1/TiO_2(101)$ surface. Distances are in Å.

Table 2 Adsorption energies and structural parameters of CO_2 adsorbed on $Pd_8/TiO_2(101)$ and $Pd_7Cu_1/TiO_2(101)$ surfaces

Configurations	C–O_a bond (Å)	C–O_b bond (Å)	O_a–C–O_b angle (°)	E_{ads} (eV)
Pd_8–CO_2	1.249	1.233	141.7	−0.58
Pd_7Cu_1–CO_2	1.281	1.249	135.9	−1.06
CO_2 molecule	1.180	1.180	180.0	

Pd_7Cu_1–CO_2. Other unstable adsorption configurations are shown in Fig. S5.† The most stable adsorption configuration Pd_7Cu_1–CO_2 appears at the Cu-6 site, which is assisted by nearby Pd-7 and Pd-8 atoms. In configuration Pd_7Cu_1–CO_2, the C atom of CO_2 bridges two Pd atoms (Pd-7 and Pd-8), and the Oa atom bonds to the Cu-6 atom. The bond lengths of the Oa–Cu-6, C–Pd-7, and C–Pd-8 bonds are 1.975 Å, 2.093 Å, and 2.127 Å, respectively. This configuration has a high exothermic adsorption energy of −1.06 eV. According to Table 2, the bond lengths of C–O_a and C–O_b bonds are elongated to 1.281 Å and 1.249 Å, respectively, which are longer than those of gas-phase CO_2 molecule, and the Oa–C–Ob angles are reduced to 135.9°, indicating CO_2 is activated upon adsorption on $Pd_7Cu_1/TiO_2(101)$ surface. The Mulliken charge analysis in Table S2† shows that the adsorbed CO_2 on $Pd_7Cu_1/TiO_2(101)$ surface has a negative charge of $-0.61|e|$. This indicates that electron transfer occurs from surface to CO_2, and forms a negatively charged $CO_2^{\delta-}$ species. The LDOS in Fig. S6c† shows that the resonant peaks lie mainly in the range of −10 to 0 eV, indicating that the adsorbed CO_2 has a strong tendency to hybridize with the $Pd_7Cu_1/TiO_2(101)$ surface at lower energy levels. Moreover, it can be seen from Table 2 that the presence of monatomic Cu significantly increases the adsorption stability of CO_2. Structurally, Pd_7Cu_1–CO_2 is similar to Pd_8–CO_2 on the $Pd_8/TiO_2(101)$ surface without Cu (Fig. 4a), but its adsorption energy is more negative (the adsorption energy increases by 0.48 eV). In addition, when CO_2 adsorbs on the $Pd_8/TiO_2(101)$ surface, the Oa–Pd-6 bond distance is 2.175 Å. However, when CO_2 adsorbs on the $Pd_7Cu_1/TiO_2(101)$ surface, the bond distance of the Oa–Cu-6 is shortened to 1.975 Å. This indicates that the interaction between CO_2 and surface becomes stronger. The Mulliken charge analysis of CO_2 on $Pd_7Cu_1/TiO_2(101)$ (Table S2†) showed the largest gain of electrons, suggesting stronger formation of $CO_2^{\delta-}$ anions. This suggests that the introduction of Cu atom enhances the activation of CO_2. Thus, $Pd_7Cu_1/TiO_2(101)$ is more favorable for CO_2 adsorption and activation compared to $Pd_8/TiO_2(101)$. This conclusion is similar to our previous work, where we also found the presence of Cu atoms to promote adsorption and activation of CO_2 on $Au/TiO_2(101)$.[43] In addition, this result is in good agreement with a recent experimental report by Long *et al.*[16] who studied photocatalytic CO_2 reduction by H_2O on clean TiO_2, Pd_xCu_1–TiO_2 ($x = 1, 3, 5, 7, 9, 11$), and Pd–TiO_2. They found that the Pd_xCu_1 alloys with isolated Cu atoms in Pd lattice can provide highly active sites to enhance the adsorption and activation of CO_2.

3.4. Dissociation of CO_2 over $Pd_8/TiO_2(101)$ and $Pd_7Cu_1/TiO_2(101)$

Having elucidated the adsorption and activation of CO_2, we now discuss the effect of bimetallic cocatalyst Pd–Cu on the dissociation of CO_2. There are two possible pathways for CO_2 dissociation: direct dissociation or H-assisted dissociation. Here, H comes from the dissociation of H_2O in the system, see Fig. S7.† We first study the direct dissociation path. The potential energy profiles are displayed in Fig. 5. Optimized structures of the transition states and products involved in this pathway are also included in Fig. 5. Starting from Pd_8–CO_2, CO_2 subsequently dissociates into adsorbed CO* and O* on the $Pd_8/TiO_2(101)$ surface through the transition state TS1. Here the asterisk (*) indicates an adsorbed species. As represented by the black line in Fig. 5, this process is endothermic by 1.44 eV and has an activation barrier of 2.80 eV. Finally, the CO* can be hydrogenated to HCO* *via* a C–H bond formation (see Fig. S8†) or desorbs from the surface into the gas phase with a heat of 0.28 eV needed to fulfill this process (see Fig. 5). And at the same time, the O* may migrate to surface oxygen vacancy (one of the most common defects in metal oxides) and becomes lattice oxygen or combine with H* in the system to form surface hydroxyl groups (OH*). For CO_2 dissociation on the $Pd_7Cu_1/TiO_2(101)$ surface (the red line in Fig. 5), beginning with Pd_7Cu_1–CO_2, the adsorbed CO_2 dissociated into CO* and O* crosses a barrier of 2.18 eV and is endothermic by 0.59 eV. Then, CO* desorption or further hydrogenation to generate HCO*. Therefore, from the viewpoint of activation barrier and reaction energy, the $Pd_7Cu_1/TiO_2(101)$ surface is more favorable for CO_2 direct dissociation than the $Pd_8/TiO_2(101)$ surface, both kinetically and thermodynamically.

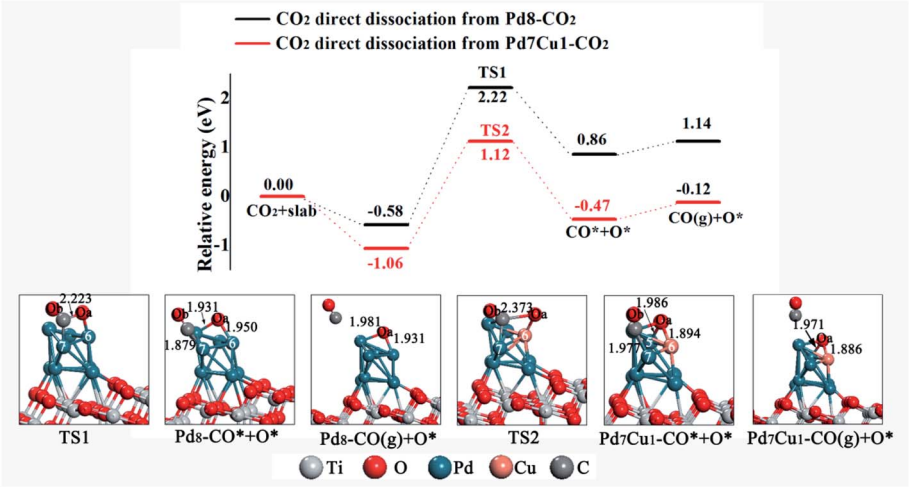

Fig. 5 Potential energy profile for the direct dissociation of CO_2 on the $Pd_8/TiO_2(101)$ and $Pd_7Cu_1/TiO_2(101)$ surfaces. Distances are in Å.

Next, we study the H-assisted CO_2 dissociation. The existence of the H atom may activate CO_2 *via* formation of COOH* or HCOO* species, which will alter the potential of CO_2 dissociation. We started with the most stable adsorption configurations Pd_8–CO_2 and Pd_7Cu_1–CO_2 and placed an H atom on the Pd-5 and Pd-8 site. For COOH* formation, the structural tends to form the *cis*-COOH* (the formation of *trans*-COOH* is shown in Fig. S9†), in which the H atom attack the Oa atom of CO_2 to form an Oa–H bond, as shown in Fig. 6. On $Pd_8/TiO_2(101)$ surface, the potential energy profile in Fig. 6 (black line) shows that the energy barrier for the first step of the *cis*-COOH* formation is 1.62 eV (TS3). This process is endothermic by 0.82 eV. Then the C–Oa band breaks and forms adsorbed CO* and OH* through the transition state TS4, with an activation barrier of 0.78 eV. This process is exothermic by 0.21 eV. Thus, the rate-determining step of this route is the process of forming *cis*-COOH*. On the $Pd_7Cu_1/TiO_2(101)$ surface, the energy profile in Fig. 6 (red line) shows that the first step of the *cis*-COOH* formation is endothermic by 0.34 eV and has an activation barrier of 1.49 eV (TS5). Then the C–Oa band breaks and forms CO* and OH* through the transition state TS6, with an activation barrier of 0.30 eV. This process is exothermic by 0.60 eV. The activation barrier of TS5 is higher than TS6, indicating that the formation of *cis*-COOH* is also the rate-determining step in this reaction. The above results for H-assisted CO_2 dissociation *via* the *cis*-COOH* path on $Pd_8/TiO_2(101)$ and $Pd_7Cu_1/TiO_2(101)$ surfaces show that the activation barrier of the rate-determining step (TS5, 1.49 eV) on the $Pd_7Cu_1/TiO_2(101)$ surface is lower than on the $Pd_8/TiO_2(101)$ surface (TS3, 1.62 eV). Moreover, the corresponding reaction energies are 0.97 and 0.34 eV, indicating that $Pd_7Cu_1/TiO_2(101)$ surface is more favorable for CO_2 dissociation than $Pd_8/TiO_2(101)$ surface. Therefore, compared to the $Pd_8/TiO_2(101)$ surface, the H-assisted CO_2 dissociation *via* the *cis*-COOH* path on the $Pd_7Cu_1/TiO_2(101)$ surface is more favorable both kinetically and thermodynamically. This result indicates that the presence of Cu-6 atom promotes the H-assisted CO_2 dissociation process.

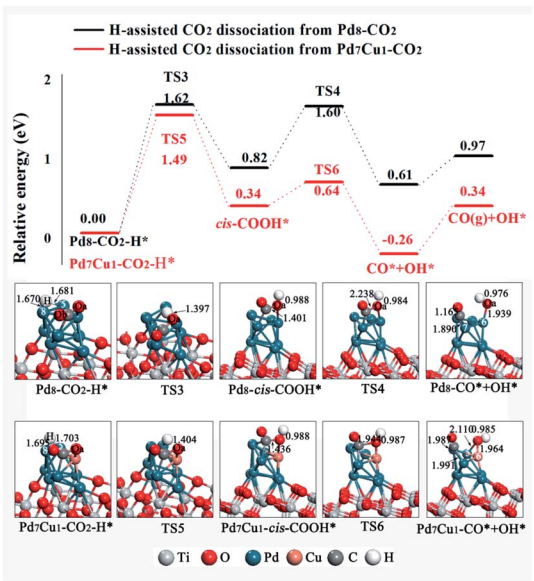

Fig. 6 Potential energy profile for the H-assisted dissociation of CO_2 *via* the *cis*-COOH* path on the $Pd_8/TiO_2(101)$ and $Pd_7Cu_1/TiO_2(101)$ surfaces. Distances are in Å.

As for HCOO* formation, the H atom attack the C atom of CO_2 to form an C–H bond, as shown in Fig. 7. On $Pd_8/TiO_2(101)$ surface, a stable bidentate HCOO* configuration was found, in which the two O atoms bond to surface Pd-6 and Pd-7, respectively. CO_2 hydrogenation to HCOO* requires surmounting a barrier of 1.45 eV, and the reaction is 0.13 eV endothermic. Next, the HCOO* cleaves to form HCO* and O* in a 1.27 eV endothermic step with 2.84 eV energy barrier, limiting the rate of reaction. Then the H atom of HCO* combine with O* and C–H band breaks to form CO* and OH* with an energy barrier of 1.85 eV and reaction energy of 0.99 eV. Finally, CO* desorption or further hydrogenation to generate HCO*. On the $Pd_7Cu_1/TiO_2(101)$ surface, the energy profile in Fig. 7 (red line) shows that the first step of the HCOO* formation is endothermic by 0.08 eV and has an activation barrier of 1.24 eV. Subsequently, the C–Oa band breaks and forms HCO* and O*

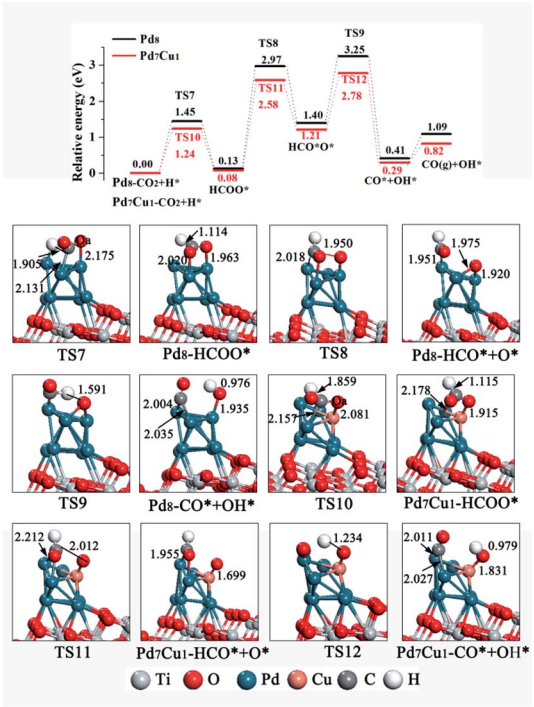

Fig. 7 Potential energy profile for the H-assisted dissociation of CO_2 *via* the HCOO* path on the $Pd_8/TiO_2(101)$ and $Pd_7Cu_1/TiO_2(101)$ surfaces. Distances are in Å.

through the transition state TS11, with an activation barrier of 2.50 eV. This process is endothermic by 1.13 eV. Then the H atom of HCO* combine with O* and C–H band breaks to form CO* and OH* with an energy barrier of 1.57 eV and reaction energy of 0.92 eV. Finally, CO* desorption or further hydrogenation to generate HCO*. This result for H-assisted CO_2 dissociation *via* the HCOO* path on $Pd_8/TiO_2(101)$ and $Pd_7Cu_1/TiO_2(101)$ surfaces show that the activation barrier of the rate-determining step on the $Pd_7Cu_1/TiO_2(101)$ surface is lower than on the $Pd_8/TiO_2(101)$ surface (2.50 *vs.* 2.84 eV). Moreover, the corresponding reaction energies are 1.09 and 0.82 eV, indicating that $Pd_7Cu_1/TiO_2(101)$ surface is more favorable for CO_2 dissociation than $Pd_8/TiO_2(101)$ surface. Therefore, compared to the $Pd_8/TiO_2(101)$ surface, the H-assisted CO_2 dissociation *via* the HCOO* path on the $Pd_7Cu_1/TiO_2(101)$ surface is also more favorable both kinetically and thermodynamically, indicating that the presence of Cu-6 atom promotes the H-assisted CO_2 dissociation process. In addition, compared to the COOH*-mediated route, HCOO*-mediated path is less competitive because of its higher barrier (2.84 and 2.50 *vs.* 1.62 and 1.49 eV). Combined with CO_2 adsorption and activation over $Pd_8/TiO_2(101)$ and $Pd_7Cu_1/TiO_2(101)$ surfaces, we can conclude that the catalytic activity of the $Pd_7Cu_1/TiO_2(101)$ is higher than that of $Pd_8/TiO_2(101)$.

3.5. Discussion

We have studied adsorption, activation, and dissociation of CO_2 over Pd–Cu supported on $TiO_2(101)$. In this section, the enhancing effect of the Cu on the catalytic activity of the Pd

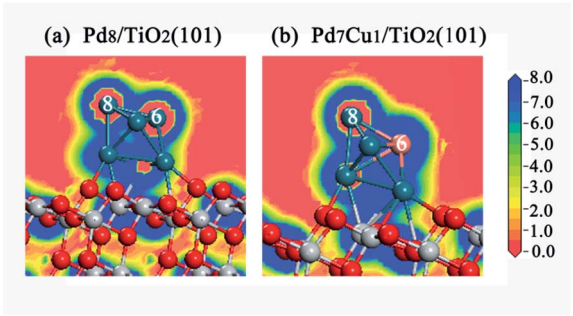

Fig. 8 The 2D electric potential maps for the (a) $Pd_8/TiO_2(101)$ and (b) $Pd_7Cu_1/TiO_2(101)$ surfaces.

supported $TiO_2(101)$ is discussed. It is a well-known fact that in addition to the surface atomic structure, the surface electronic states are also closely related to the catalytic activity. Therefore, in order to determine the intrinsic factors that promote the catalytic activity of $Pd_7Cu_1/TiO_2(101)$, a detailed comparison of the surface electronic states between the surfaces of $Pd_8/TiO_2(101)$ and $Pd_7Cu_1/TiO_2(101)$ was conducted.

As shown in Fig. 8, the 2D electric potential maps of $Pd_7Cu_1/TiO_2(101)$ shows that the electric potential distribution on the Cu-6 and Pd-8 atoms is no longer uniform due to the large charge polarization between Cu-6 and Pd atoms. The positive polarization potential of the Cu-6 atom is higher than that of the Pd-8 atom. This means that the electric field on the Cu-6 atom is higher than that on the Pd-8 atom. This response can promote the adsorption of CO_2 (in which the O atoms are negatively charged) by increasing the electrostatic attraction between the CO_2 and the Cu-6 atom. Therefore, the surface activity of the $Pd_7Cu_1/TiO_2(101)$ is improved compared to the $Pd_8/TiO_2(101)$,

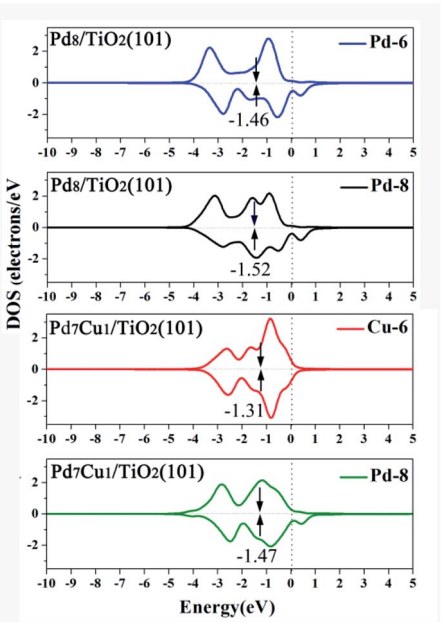

Fig. 9 Projected d-band states of Pd and Cu on the $Pd_8/TiO_2(101)$ and $Pd_7Cu_1/TiO_2(101)$ surfaces. The d-band center is marked by black arrow. The Fermi level is set to 0 eV.

and the active center is the introduced Cu atom. It is precisely because of the stable adsorption of CO_2 on Cu-6 atoms and the special electric field on Cu-6 atoms that the reactivity of CO_2 is enhanced. This result is consistent with previous results. Jia *et al.*[44] investigated the CO oxidation on Ru–Pt supported on TiO_2(101) and found that the special electric field on the top-layered Ru atom can enhance the stability and reactivity of CO + O_2. Luo *et al.*[45] reported that the optimal performance shows a strong dependence on the interaction between CO_2 and the local electric field.

Fig. 9 is DOS projected onto the d orbitals of Pd-6 (or Cu-6) and Pd-8 on the Pd_8/TiO_2(101) and Pd_7Cu_1/TiO_2(101) surfaces. It can be seen from the Fig. 9 that the d-band center (ε_d) of the Cu-6 atom on Pd_7Cu_1/TiO_2(101) is higher than that of the Pd-6 atom on Pd_8/TiO_2(101) (−1.31 *versus* −1.46 eV). It is a well-known fact that, relative to the Fermi level, the higher the energy of the d-band states, the stronger the interaction with the adsorbate.[46] This is because when the d-band states is close to the Fermi level, the antibonding states can be pushed above the Fermi level.[46] Therefore, Pauli repulsion decreases and the binding strength between the adsorption site and adsorbate increases.[46] Thus, the adsorption strength of CO_2 on Pd_7Cu_1/TiO_2(101) surface is higher than that of Pd_8/TiO_2(101) surface. Our results are consistent with previous results that show the adsorption strength of CO_2 is controlled by the d-band center of the metal surfaces. For example, Long *et al.*[16] calculated the d-band centers of Cu atom in Pd_7Cu_1 and Pd_1Cu_1 lattices, and found that the Cu d-band center of Pd_7Cu_1 lattice is significantly higher than that of Pd_1Cu_1 lattice (−1.161 *versus* −1.452 eV), and the adsorption energy of CO_2 on Pd_7Cu_1 lattice is stronger than that on Pd_1Cu_1 lattice (−0.463 *versus* −0.308 eV).

Based on the above discussion, the following conclusions can be drawn: due to the strong positive polarization potential and the elevated Cu d-band center, the Pd_7Cu_1/TiO_2(101) has high activity, which promotes CO_2 adsorption and dissociation.

4. Conclusions

In order to understand the origin of the activity of Pd–Cu bimetallic nanoclusters supported on TiO_2(101), adsorption, activation, and dissociation of CO_2 on TiO_2-supported Pd and Pd–Cu clusters were investigated using DFT calculation. The results show that the activity of Pd_7Cu_1/TiO_2(101) can be greatly improved by introducing Cu atom. Because of the significant charge polarization between the Cu atom and the neighboring Pd atoms on the Pd_7Cu_1/TiO_2(101) surface, the positive polarization potential of the Cu atom is much higher than that of the Pd atom. This response can promote the adsorption of CO_2 by increasing the electrostatic attraction between CO_2 and the Cu site. Meanwhile, the elevated Cu d-band center on the surface of Pd_7Cu_1/TiO_2(101) would increase its surface catalytic activity. Therefore, compared to Pd_8/TiO_2(101) surface, the activity of Pd_7Cu_1/TiO_2(101) surface is higher, and the active center is the introduced Cu atom. This result is not only immensely helpful for the development of effective CO_2 photocatalysts, but also essential for understanding the basic mechanisms of bimetallic catalysis.

Conflicts of interest

There are no conflicts to declare.

Acknowledgements

This research was supported by the Foundation (No. ZZ20200133) of State Key Laboratory of Biobased Material and Green Papermaking, Qilu University of Technology (Shandong Academy of Sciences) and the Natural Science Foundation of Shandong Province of China (Grant No. ZR2018LA013).

References

1 K. Li, B. Peng and T. Peng, *ACS Catal.*, 2016, **6**, 7485–7527.
2 V. P. Indrakanti, J. D. Kubicki and H. H. Schobert, *Energy Environ. Sci.*, 2009, **2**, 745–758.
3 A. Dhakshinamoorthy, S. Navalon, A. Corma and H. Garcia, *Energy Environ. Sci.*, 2012, **5**, 9217–9233.
4 W. Chu, Q. Zheng, O. V. Prezhdo and J. Zhao, *J. Am. Chem. Soc.*, 2020, **142**, 3214–3221.
5 S. Navalón, A. Dhakshinamoorthy, M. Álvaro and H. Garcia, *ChemSusChem*, 2013, **6**, 562–577.
6 Y. Izumi, *Coord. Chem. Rev.*, 2013, **257**, 171–186.
7 S. N. Habisreutinger, L. Schmidt-Mende and J. K. Stolarczyk, *Angew. Chem., Int. Ed.*, 2013, **52**, 7372–7408.
8 S. C. Roy, O. K. Varghese, M. Paulose and C. A. Grimes, *ACS Nano*, 2010, **4**, 1259–1278.
9 X. Chen and S. S. Mao, *Chem. Rev.*, 2007, **107**, 2891–2959.
10 A. Kubacka, M. Fernandez-Garcia and G. Colon, *Chem. Rev.*, 2012, **112**, 1555–1614.
11 Ș. Neațu, J. A. Maciá-Agulló, P. Concepción and H. Garcia, *J. Am. Chem. Soc.*, 2014, **136**, 15969–15976.
12 D. Tan, J. Zhang, J. Shi, S. Li, B. Zhang, X. Tan, F. Zhang, L. Liu, D. Shao and B. Han, *ACS Appl. Mater. Interfaces*, 2018, **10**, 24516–24522.
13 X. Li, J. Yu, M. Jaroniec and X. Chen, *Chem. Rev.*, 2019, **119**, 3962–4179.
14 V. Vaiano, D. Sannino and P. Ciambelli, *Photochem. Photobiol. Sci.*, 2015, **14**, 550–555.
15 Y. Zhang, X. Wang, P. Dong, Z. Huang, X. Nie and X. Zhang, *RSC Adv.*, 2018, **8**, 15991–15998.
16 R. Long, Y. Li, Y. Liu, S. Chen, X. Zheng, C. Gao, C. He, N. Chen, Z. Qi, L. Song, J. Jiang, J. Zhu and Y. Xiong, *J. Am. Chem. Soc.*, 2017, **139**, 4486–4492.
17 Y. Wang, Q. Lai, F. Zhang, X. Shen, M. Fan, Y. He and S. Ren, *RSC Adv.*, 2014, **4**, 44442–44451.
18 L. Liu, Z. Liu, H. Sun and X. Zhao, *Appl. Surf. Sci.*, 2017, **399**, 469–479.
19 X. Zhang, F. Han, B. Shi, S. Farsinezhad, G. P. Dechaine and K. Shankar, *Angew. Chem., Int. Ed.*, 2012, **51**, 12732–12735.
20 S. Lee, S. Jeong, W. D. Kim, S. Lee, K. Lee, W. K. Bae, J. H. Moon, S. Lee and D. C. Lee, *Nanoscale*, 2016, **8**, 10043–10048.
21 Q. Kang, T. Wang, P. Li, L. Liu, K. Chang, M. Li and J. Ye, *Angew. Chem., Int. Ed.*, 2015, **54**, 841–845.

22 M. Tahir, B. Tahir and N. A. S. Amin, *Appl. Catal., B*, 2017, **204**, 548–560.
23 Q. Chen, X. Chen, M. Fang, J. Chen, Y. Li, Z. Xie, Q. Kuang and L. Zheng, *J. Mater. Chem. A*, 2019, **7**, 1334–1340.
24 J. Jiao, Y. Wei, Y. Zhao, Z. Zhao, A. Duan, J. Liu, Y. Pang, J. Li, G. Jiang and Y. Wang, *Appl. Catal., B*, 2017, **209**, 228–239.
25 S. Bai, Q. Shao, P. Wang, Q. Dai, X. Wang and X. Huang, *J. Am. Chem. Soc.*, 2017, **139**, 6827–6830.
26 Y. Yang and D. Cheng, *J. Phys. Chem. C*, 2014, **118**, 250–258.
27 M. C. Payne, M. P. Teter, D. C. Allan, T. A. Arias and J. D. Joannopoulos, *Rev. Mod. Phys.*, 1992, **64**, 1045–1097.
28 J. P. Perdew, J. A. Chevary, S. H. Vosko, K. A. Jackson, M. R. Perderson, D. J. Singh and C. Fiolhais, *Phys. Rev. B: Condens. Matter Mater. Phys.*, 1992, **46**, 6671–6687.
29 J. P. Perdew, J. A. Chevary, S. H. Vosko, K. A. Jackson, M. R. Perderson, D. J. Singh and C. Fiolhais, *Phys. Rev. B: Condens. Matter Mater. Phys.*, 1993, **48**, 4978.
30 J. P. Perdew, K. Burke and Y. Wang, *Phys. Rev. B: Condens. Matter Mater. Phys.*, 1996, **54**, 16533–16539.
31 J. P. Perdew, K. Burke and Y. Wang, *Phys. Rev. B: Condens. Matter Mater. Phys.*, 1998, **57**, 14999.
32 M. Segall, P. Lindan, M. Probert, C. Pickard, P. Hasnip, S. Clark and M. Payne, *J. Phys.: Condens. Matter*, 2002, **14**, 2717–2744.
33 D. Vanderbilt, *Phys. Rev. B: Condens. Matter Mater. Phys.*, 1990, **41**, 7892–7895.
34 H. J. Monkhorst and J. D. Pack, *Phys. Rev. B: Solid State*, 1976, **13**, 5188–5192.
35 T. A. Halgren and W. N. Lipscomb, *Chem. Phys. Lett.*, 1977, **49**, 225–232.
36 C.-T. Yang, B. C. Wood, V. R. Bhethanabotla and B. Joseph, *J. Phys. Chem. C*, 2014, **118**, 26236–26248.
37 Y. Han, M. Zhang, W. Li and J. Zhang, *Phys. Chem. Chem. Phys.*, 2012, **14**, 8683–8692.
38 C. T. Yang, B. C. Wood, V. R. Bhethanabotla and B. Joseph, *Phys. Chem. Chem. Phys.*, 2015, **17**, 25379–25392.
39 D. C. Sorescu, W. A. Al-Saidi and K. D. Jordan, *J. Chem. Phys.*, 2011, **135**, 124701.
40 J. X. Liu, Y. Su, I. A. W. Filot and E. J. M. Hensen, *J. Am. Chem. Soc.*, 2018, **140**, 4580–4587.
41 Y. Li, C. Liu, Z. Pu, L. Bao, Y. Zhu and J. Ma, *J. Phys. Chem. C*, 2019, **123**, 13739–13747.
42 H. J. Freund and M. W. Roberts, *Surf. Sci. Rep.*, 1996, **25**, 225–273.
43 L. Liu and P. Lv, *New J. Chem.*, 2020, **44**, 14662–14669.
44 C. Jia, W. Zhong, M. Deng and J. Jiang, *J. Chem. Phys.*, 2018, **148**, 124701.
45 H. Jiang, Z. Hou and Y. Luo, *Angew. Chem., Int. Ed.*, 2017, **56**, 15617–15621.
46 J. Xiao and T. Frauenheim, *J. Phys. Chem. C*, 2013, **117**, 1804–1808.